

## Decoding groundwater salinity using hydrochemical and isotopic techniques: A case study for Abulug River Basin, Philippines

C.B. Mata<sup>1,2\*</sup>, L.A. Alejo<sup>3</sup>, O.F. Balderama<sup>3</sup>, J.L.R. Bareng<sup>3</sup>, T.J.A. Mata<sup>2</sup>, C.D.T. Racadio<sup>4</sup>

<sup>1</sup>*Isabela State University, San Fabian, Echague, Isabela, Philippines*

<sup>2</sup>*Research Directorate, Mariano Marcos State University, Quiling Sur, Batac City, Ilocos Norte, Philippines*

<sup>3</sup>*College of Engineering, Isabela State University, San Fabian, Echague, Isabela, Philippines*

<sup>4</sup>*Philippine Nuclear Research Institute, Department of Science and Technology, Commonwealth Ave., Diliman, Quezon City, Philippines*

Received 28 July 2025; Received in revised form 25 February 2026; Accepted 14 April 2026

### ABSTRACT

Despite increasing evidence of groundwater salinization, the processes driving it and its geographic extent in the Abulug River Basin remain unexamined. Although complex methods exist, this study demonstrates that a simplified approach can yield meaningful insights into hydrological processes in the basin by combining findings from hydrochemical analysis, isotope techniques, and GIS mapping. Thirty-two sampling sites yielded 96 samples. Most of the samples exhibited similar behavior, except for a few. While the majority of the well samples in the research area are classified as Ca-Mg-HCO<sub>3</sub>, a recently formed groundwater with a short average residency period recharged by precipitation, a few samples exhibited the Na-Cl water type, which typically denotes salinization. Two river samples and seven well samples are within the mixing line. These samples are identified using the results from several ionic elements, ratios, and isotopic composition. Evolution diagrams, such as the Gibbs, Chadha, and Piper diagrams, suggested that seawater intrusion was not the only cause of salinization. The groundwater quality in the basin's coastal aquifer is deteriorating due to dominant salinization drivers, including seawater intrusion, paleo-saline groundwater, and rock-water interactions such as cation exchange, silicate weathering, and halite dissolution. It is recommended to prioritize policy implications for local managers, such as abstraction limits, integration of geophysical surveys, and sentinel network monitoring.

*Keywords:* Abulug River Basin, Philippines, coastal aquifer, ionic ratio, seawater intrusion, stable isotopes.

### 1. Introduction

Numerous studies in coastal aquifers have concentrated on saltwater intrusion as the cause of groundwater (Hajji et al., 2022; Prusty & Farooq, 2020). Although recognized as the principal factor contributing to groundwater salinization in coastal aquifers, other potential sources of saltwater

contamination exist that are not related to seawater intrusion. Aquifers near the coast are vital water sources and can be affected by a variety of land-use practices and geochemical contaminants (Rajendiran et al., 2021). Seawater intrusion, rock-water interaction, excessive groundwater pumping, rising sea level, hydrogeological history of the area, and anthropogenic activities are among the most commonly identified factors that can

\*Corresponding author, Email: [cbmata@mmsu.edu.ph](mailto:cbmata@mmsu.edu.ph)

influence groundwater salinization (Anders et al., 2014; Rajendiran et al., 2021).

Abulug River Basin (ARB) is located in the northern most of Luzon, Philippines that covers the provinces of Apayao in the Cordillera and Cagayan Valley in Region 2 (Fig. 1). The ARB is one of the nation's 18 principal river basins that the Department of Environment and Natural Resources' River Basin Control Office (DENR-RBCO) has designated as a priority region for sustainable resource management and development. It has been the focus of an integrated area development study, which follows the framework for resource management of coastal areas and watersheds.

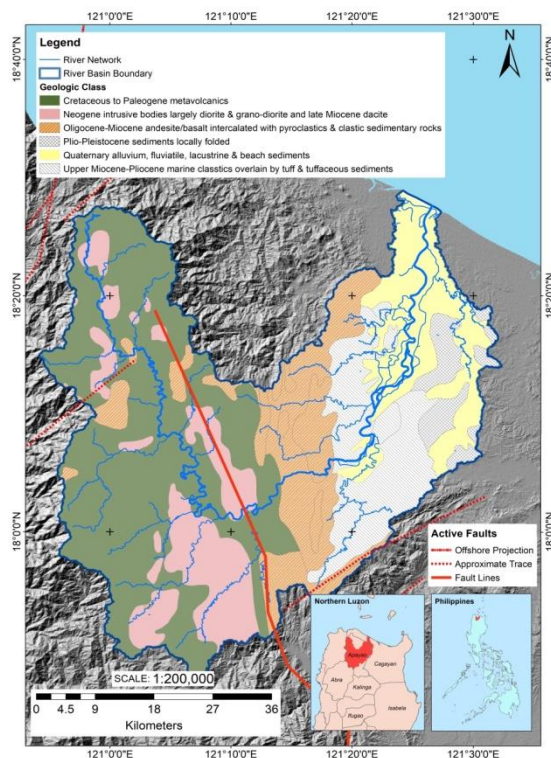


Figure 1. Geospatial locations of the Abulug River Basin in the Northern Philippines and sampling points before and during the Northeast Monsoon

In Cagayan Valley, which covers the coastal portion of ARB, groundwater salinity was first studied and measured in 2017 by the

Department of Agriculture Bureau of Soils and Water Management (DA-BSWM) based solely on electrical conductivity to investigate rice suitability. The report also mentioned that it is likely caused by several factors, including sea level rise, excessive groundwater abstraction or seepage, or tidal flooding along rivers, which occurs when seawater flows upstream into rivers during high tide and low river flow. Given the multiple factors mentioned above, understanding the cause of salinization in specific areas is challenging. The existing literature in the study area is scarce, with only one previous study to date (DA-BSWM, 2017), and the spatial extent and specific driving mechanisms are limited, which has limited its conclusions.

Groundwater-dependent agriculture is one of the principal land-use patterns in the downstream of ARB, where groundwater serves as the primary water source for both domestic and agricultural needs. In this coastal setting, intensive groundwater abstractions promote landward migration of the groundwater-seawater interface, leading to aquifer salinization (Rajendiran et al., 2021). The downstream of ARB is characterized by a coastal, active tidal-flat estuarine plain that is frequently inundated during high tides and elevated sea levels, particularly when combined with prolonged or high-intensity rainfall events. Soils in this area are predominantly fine loamy to clayey, exhibit moderate to deep salinity saturation, and are extremely poorly drained, conditions that further enhance salt accumulation.

Under these circumstances, salinization can be attributed to one or a combination of the factors presented above. These alarming problems, exacerbated by climate change, require urgent action to make groundwater mechanisms visible in an unobstructed, simple, fast, and easy way (Kärnä et al., 2015). While previous hydrogeological studies in the southern and central part of the

Philippines, particularly Pampanga (Tan et al., 2020; Torres et al., 2011) and Boracay Island (Valdez et al., 2026) have extensively documented the vulnerability of coastal aquifers to saltwater intrusion and several salinity-influencing factors, the coastal aquifers of Northern Luzon remain comparatively unexplored, leaving a significant data gap in the characterization of groundwater salinization mechanisms within the Abulug River Basin. This study tests the hypothesis that groundwater salinization is not solely a result of saltwater intrusion but a multi-causal process. To determine groundwater salinity and to assess the dominant hydrochemical processes contributing to salinization, isotope tracing and hydrogeochemical analysis were performed. Hydrochemical parameters, ionic ratio, water stable isotopes ( $\delta^{18}\text{O}$  and  $\delta\text{D}$ ), and mapping using GIS were assessed. Despite the recognized importance of groundwater in ARB, there is a clear gap in the literature for properly assessing groundwater salinization mechanisms at the study site and making recommendations for sustainability.

## 2. Study Area

Numerous faults and folds are indicative of the area's geomorphologic evolution, as shown in Fig. 1. One of the main factors influencing the Philippine Fault Zone is the Bangui Fault System, which extends upstream of the River Basin. The western part, on the other hand, is influenced by the West Ilocos Fault System, while the Dummon River Fault System influences the eastern part.

The general geologic structure of the ARB is complex. Based on the Mines and Geosciences Bureau's (MGB) classification, the basin is dominated by igneous volcanic formations (48.66%; 1,379.7 km<sup>2</sup>) and sedimentary formations (37.65%; 1,067.5 km<sup>2</sup>). According to the RBCO (2014) investigative report, most sedimentary

formations are located at low elevations. They are composed of Quaternary alluvium, fluvial, lacustrine, and beach sediments, as well as locally folded sediments. The predominance of these unconsolidated and semi-consolidated materials in the basin's downstream sections contributes to high aquifer permeability but also renders the groundwater system vulnerable to salinization under conditions of seawater intrusion and anthropogenic stress.

In comparison, igneous volcanic formations, diorite intrusion, and other geologic processes that raised the entire basin are drawn to the area upstream by igneous volcanic formations and faults. These areas are composed of marine clastics overlain by tuff and tuffaceous sediments. The Cretaceous Paleogene, the oldest rocks in Apayao, which cover most of the mountainous parts, consists of undifferentiated volcanic flows with regionally intercalated sedimentary strata.

Within the ARB, groundwater occurs primarily in unconsolidated alluvial and coastal sediment aquifers that are typical of lowland fluvial and tidal-plain environments. These aquifers consist of Quaternary alluvium, composed of sands, gravels, silts, and clays, forming unconfined to semi-confined intergranular aquifer systems that yield groundwater for domestic and agricultural use. Groundwater flow in such systems is predominantly through the pore spaces of unconsolidated sediments, with permeability varying with grain size and sediment sorting. In coastal portions of the basin, aquifers are subject to interaction with seawater, creating transitional freshwater-brackish zones that reflect coastal unconfined aquifer conditions influenced by saltwater intrusion processes. The broader Cagayan Valley aquifer system, which includes the coastal area of ARB, has been conceptualized in hydrogeological studies in the Philippines as comprising extensive intergranular aquifers

of high to moderate productivity underlain by less permeable units, with groundwater flow largely controlled by sediment distribution and recharge from rainfall and surface water bodies (NEDA, 2026). However, it should be noted that the hydrogeological model presented here is inferred from regional geological proxies and the NEDA (2026) Cagayan Valley framework, and is not derived from site-specific borehole logs.

### 3. Methodology

#### 3.1. Sample collection

##### 3.1.1. Sampling of groundwater and surface water

Groundwater samples were collected in the northern coastal region of ARB (Fig. 2). Samples were collected in November 2022 and April 2023, before and during the Northeast Monsoon, respectively. Pre-monsoon sampling was exploratory and limited to a small number of sites comprising three coastal wells, seawater, and a nearby river adjacent to the wells, with analysis restricted to pH, EC,  $\text{HNO}_3^-$ , and  $\text{NO}_3^-$ , and isotopic variations. These data served as baseline information and guided the design of the monsoon sampling strategy. As such, the study does not aim to provide a detailed comparison between seasons; instead, the analyses focus on the monsoon dataset to determine spatial extent and processes of groundwater salinization. A few surface water samples from the Abulug River: upstream, midstream, and downstream were collected to determine the geographical variation of parameters. Moreover, a few rivers that diverge from the Abulug River, such as the Tautit River and the Guiddam River, and one irrigation canal were sampled to assess surface-water mixing. Water samples from brackish water near both the coastline and production wells were likewise collected.

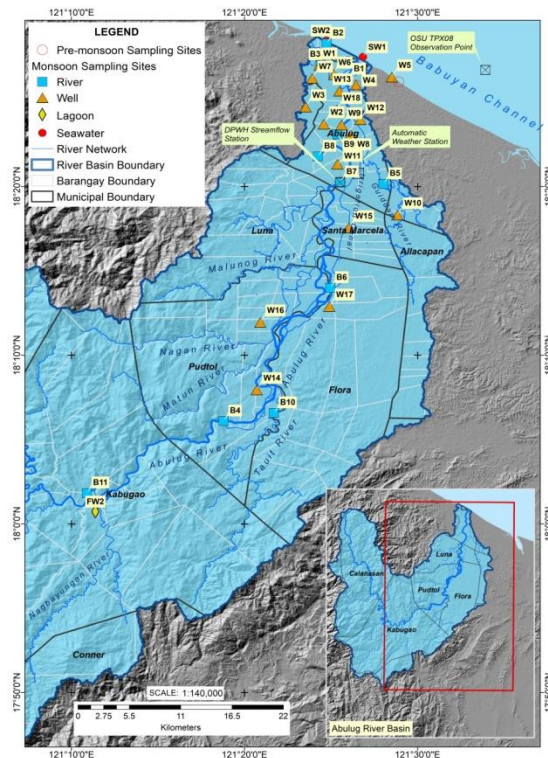


Figure 2. Geology map of Abulug River Basin

Furthermore, seawater (end members) and rainwater were sampled as well to determine the origin of salinity. The sampling for production wells, on the other hand, was arranged in perpendicular transects with sampling intervals of 750 m from the coast and horizontal distances of 5000 m, placed alternately. This method, called staggered grids or systematic sampling, yielded the lowest actual prediction errors (APE) in the comparative study conducted by Ohmer et al. (2019), which compared random, geostatistical, and spatial coverage sampling to optimize monitoring well placement and achieve better spatial coverage with fewer wells. The interpolation results, however, are most robust in the basin's alluvial plain, where sampling sites are most numerous to capture the spatial variability of the saltwater-freshwater interface. In the upstream regions, interpolation helps characterize the isotopic continental effect and the broad regional

transition toward a meteoric-dominated regime. Sampling density and spacing were primarily determined by site accessibility and local administrative constraints. This study serves as a pilot to justify the installation of a dedicated groundwater monitoring network and subsequent geophysical surveys. Overall, sampling sites were strategically arranged to better understand the extent and sources of groundwater salinization in the basin. Eleven rivers, two seawaters, one lagoon, and 18 groundwater samples were sampled in total. Groundwater samples were collected from active production wells.

Water samples were collected at each site and placed in four distinct, sterile, high-density polypropylene bottles: two 500 mL bottles (one for anions and one for cations), and one 60 mL bottle for isotope analysis. Following a 24-hour immersion in a 1:1 HCl solution, the sampling bottles were cleaned with deionized water and dried in an oven. The majority of the samples came from dug wells for home or agricultural use.

The Horiba multi-parameter probe (Model U-50) was used to measure in situ the

physical parameters, including pH, electrical conductivity (EC), total dissolved solids (TDS), dissolved oxygen (DO), and temperature. Using a digital titration (Hach) and a portable nitrate meter, bicarbonate and Nitrate were measured three (3) times in situ. Digital arsenator (Palintest) was used to measure arsenic concentrations in all samples. To guarantee consistency in data quality, sample collection, handling, preservation, and analysis were carried out in accordance with the IAEA (International Atomic Energy Agency, 2007) standard procedures.

### 3.1.2. Collection of rainwater

The total monthly precipitation was collected using two types of collectors and measured for one year from October 2022 to September 2023 (Fig. 3). The step-by-step procedure for the construction of an improvised rainwater collector is documented by Racadio et al. (2020). Bottles of 1-L or 500-mL HDPE rainwater were collected monthly and sent to the Philippine Nuclear Research Institute (PNRI) for isotopic analysis. For comparison, monthly precipitation recorded by AWS at the same compound was also graphed.

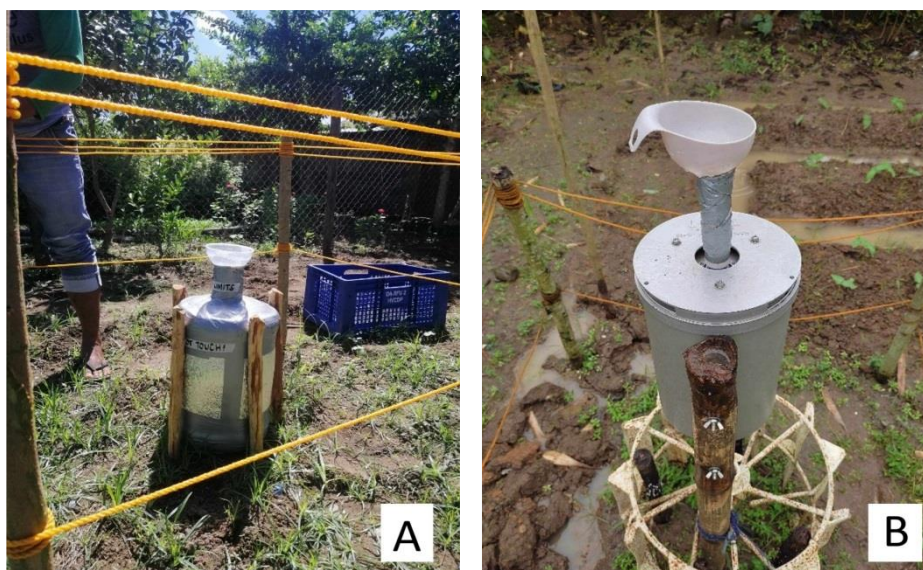


Figure 3. (A) Improvised rainwater collector for October to December 2021 and (B) Palmex Rain Sampler RS1 for January to September 2022

### 3.2. Data Analysis

#### 3.2.1. Hydrochemical evaluation methods

Major anions ( $\text{SO}_4^{2-}$ ,  $\text{Cl}^-$ ), minor anion ( $\text{Br}^-$ ), and major cations ( $\text{Na}^+$ ,  $\text{Ca}^{2+}$ ,  $\text{Mg}^{2+}$ ,  $\text{K}^+$ ) were analyzed using various standard techniques in accordance with Standard Method for the Examination of Water and Wastewater (APHA, 2017) protocols. The ability to distinguish between freshwater and saltwater is aided by the concentration of these ionic elements in water samples. Using graphical plots and statistical analyses, 13 physical and chemical parameters, as well as arsenic and water stable isotopes ( $\delta^{18}\text{O}$  and  $\delta\text{D}$ ), were analyzed. By calculating the ion balance error, which was within 5%, the analytical precision of the measured ion was ascertained.

The primary methods utilized in the interpretation process are graphical illustration techniques such as Piper diagram based on Stosch (Stosch, 2022), Chadha's diagram (Chadha, 1999), Gibb's scatter plots (Gibbs, 1970), the computation of Simpson ionic ratio as suggested by (Todd and Mays, 2005) in relation to geological characteristics of the basin, and the development of hydrochemical variation maps. These visuals show the spatial variation in water quality parameters across the study area using inverse distance weighting (IDW) interpolation.

#### 3.2.2. Stable isotopic techniques to analyze groundwater salinization

The Los Gatos Research Liquid Water Isotope Analyzer (LWIA) 45EP was used to measure stable isotopes of oxygen and hydrogen. It is connected to a CTC PAL LC xt autosampler through a PTFE transfer line. For  $\delta^{18}\text{O}$  and  $\delta\text{D}$ , the analytical error is within 0.2 and 1.5‰, respectively.

Following the conversion of molecular concentrations into atomic ratios,  $2\text{H}/1\text{H}$  and  $^{18}\text{O}/^{16}\text{O}$ , the following formula was used to determine the delta ( $\delta$ ) values in units per mill (‰) in relation to the Vienna Standard Mean Ocean Water (VSMOW) standard:

$$\delta(\text{‰}) = \frac{R_{\text{measured}} - R_{\text{VSMOW}}}{R_{\text{VSMOW}}} \times 1000$$

where  $R$  is the isotopic ratio of  $2\text{H}/1\text{H}$  and  $^{18}\text{O}/^{16}\text{O}$ . The heavier isotope is higher or "enriched" if the -value is more positive than the reference isotope, whereas the heavier isotope is less or "depleted" if the -value is more negative.

Groundwater samples were analyzed for stable isotopes ( $\delta^{18}\text{O}$  and  $\delta\text{D}$ ) and plotted as  $\delta^{18}\text{O}$  vs.  $\delta\text{D}$ , which provides a diagnostic indicator of the hydrologic processes that formed the groundwater. A weighted average of the stable-isotopic composition of the collected precipitation was used to calculate the initial composition. Following an evaluation of the isotopic signature's evolution from upstream to downstream, river samples were compared with shallow-well and rainfall samples.

## 4. Results and Discussion

### 4.1. Distribution of Ions

At a small number of well-sampling sites, the region uses groundwater for drinking; thus, the desirability of the groundwater for this purpose was compared with drinking water quality standards set by the Philippine National Standards for Drinking Water (PNSDW, 2017). The summary of hydrochemical parameters analyzed at five sampling sites during the dry season is shown in Table 1.

Freshwater usually ranges from 0 to 1,500  $\mu\text{S}/\text{cm}$ , and typical seawater has a conductivity of about 50,000  $\mu\text{S}/\text{cm}$ . According to PNSDW (2017), 2,500–10,000  $\mu\text{S}/\text{cm}$  is not recommended for human consumption, although up to 3000  $\mu\text{S}/\text{cm}$  can be consumed. It is also not normally suitable for irrigation, although up to 6,000  $\mu\text{S}/\text{cm}$  can be used only by salt-tolerant crops (Ayers & Westcot, 1985).

W1, located in an agricultural area used for rice irrigation for two cropping seasons per year, exhibited very high EC. The well is

2.55 km from the coastline, with a nearby river about 1 km away, and locals say flooding is frequent in the area. A high EC value may result from local flooding with brackish water, seawater intrusion, evaporation dominance, or

the absorption of highly concentrated ions through ionic exchange. Therefore, isotopes need to be analyzed first. In addition, more sampling sites are recommended to identify the extent and source of salinity.

Table 1. Hydrochemical data of identified wells and rivers in Abulug River Basin during the pre-monsoon (April 20, 2022)

Site No.	Date	Latitude	Longitude	pH	EC (µS/cm)	Temp (°C)	Bicarbonates (ppm)			NO <sub>3</sub> <sup>-</sup> (ppm)	δ <sup>2</sup> H (‰)	δ <sup>18</sup> O (‰)
							1	2	3			
B7	04/20/22	18.3378	121.425497	8.09	213	29.01	70	83	8.09	213	-29.8	-5.49
SW1	04/20/22	18.43695	121.481927	-	-	-	-	-	-	-	-1.9	-0.39
W1	04/20/22	18.45321	121.405746	6.53	2770	27.85	239	241	6.53	2770	-16.6	-3.22
W4	04/20/22	18.43372	121.44085	6.72	370	28.14	103	102	6.72	370	-26	-4.44
W5	04/20/22	18.44152	121.475235	8.5	704	28.93	79	83	8.5	704	-23.3	-4.6

Symbols with a hyphen (-) mean no data were gathered, whereas zero (0) means nothing is recorded

The hydrochemical and isotope data for the sampling sites during the 2022 monsoon are shown in Table 2, whereas the basic statistics of the chemical composition of groundwater sampled from wells (EC, TDS, DO, and pH) are listed in Table 3. Significant and skewed variations in most parameters indicate that several factors influence the groundwater hydrochemistry

in the region. Samples have an average pH of 6.91, suggesting groundwater that is acidic to neutral. All groundwater samples are within the suitable range of 6.5–8.5 for drinking purposes (PNSDW, 2017). In line with pH for safe drinking is the Nitrate. Three well samples, including W2, W3, and W5, were not within the suitable limit of 50.00 ppm.

Table 2. Analytical results of physiochemical and isotope parameters of identified wells and rivers in Abulug River Basin during the monsoon (November 7–10, 2022)

Source	Sample ID	Date (mm/dd/yy)	Latitude (N)	Longitude (E)	Elev. (masl)	Distance from coast (km)	pH	EC (µS/cm)	Temp (°C)	DO (mg/L)	TDS (ppm)	HCO <sub>3</sub> <sup>-</sup> (ppm)	NO <sub>3</sub> <sup>-</sup> (ppm)	Na <sup>+</sup> (ppm)	Ca <sup>2+</sup> (ppm)	Mg <sup>2+</sup> (ppm)	K <sup>+</sup> (ppm)	SO <sub>4</sub> <sup>2-</sup> (ppm)	Cl <sup>-</sup> (ppm)	Br <sup>-</sup> (ppm)	δ <sup>2</sup> H (‰)	δ <sup>18</sup> O (‰)	As (µg/L)
River	B1	11/08/22	18.43941	121.432614	1.0003	2.57	7.61	211	27.70	8.6367	137.33	81	37.91	21.6	125.0	32.6	0.32	9.34	4.9	0.06	-37.9	-6.03	0
River	B2	11/07/22	18.474722	121.412500	0.8072	0.14	6.71	1545	30.34	10.4600	1008.00	73	22.36	584.0	68.9	44.8	9.45	47.20	415.0	0.66	-38.3	-6.28	0
River	B3	11/08/22	18.453726	121.406715	3.2271	2.45	6.89	3087	27.29	9.2800	1976.67	91	18.63	1004.0	103.0	45.8	19.20	105.00	833.0	1.48	-35.7	-5.82	0
River	B4	11/09/22	18.101614	121.313189	46.5049	41.24	7.88	176	25.58	3.1833	114.33	66	45.94	18.2	75.9	31.7	0.68	13.40	0.2	0.18	-41.3	-6.93	0
River	B5	11/09/22	18.336047	121.467238	8.8825	11.40	7.52	257	28.46	10.5600	167.00	86	11.91	21.7	288.0	34.5	2.01	0.25	2.9	0.01	-34.8	-5.67	0
River	B6	11/09/22	18.233314	121.415891	7.9806	23.69	8.20	189	27.15	9.2567	122.67	70	18.27	17.6	103.0	32.9	0.05	8.24	0.2	0.01	-39	-6.19	0
River	B7	11/09/22	18.337799	121.425497	7.7714	12.53	7.85	186	27.45	11.1233	119.00	72	16.42	18.7	110.00	33.3	0.05	6.41	0.2	0.01	-38.9	-6.55	0
River	B8	11/07/22	18.363178	121.404010	13.3901	11.24	7.75	194	29.05	3.5933	126.33	71	31.34	22.4	97.0	32.2	1.14	0.25	8.8	0.01	-30.8	-6.01	0
River	B9	11/08/22	18.384972	121.422973	0.0006	8.15	7.89	216	26.85	8.9800	135.00	73	6.82	23.0	137.0	34.1	0.74	6.41	0.2	0.01	-37.4	-6.43	0
River	B10	11/09/22	18.109665	121.361635	39.7292	38.48	7.97	241	25.95	10.1833	156.33	98	16.42	15.6	216.0	33.5	0.37	1.83	2.0	0.01	-30.4	-5.91	0
River	B11	11/10/22	18.030511	121.181447	91.0037	54.94	7.89	170	25.74	9.5333	110.67	65	21.03	17.9	65.7	32.9	0.05	0.25	0.2	0.01	-42.2	-6.97	0
Lagoon	FW2	11/10/22	18.012352	121.189776	152.2198	56.20	7.38	114	29.94	6.7967	74.00	45	1.00	15.2	1238.0	23.4	0.42	0.25	0.2	0.01	-47.3	-6.91	0
Seawater	SW1	11/08/22	18.461474	121.447457	0.0030	0.00	-	-	-	-	-	100	0.10	1143.0	68.0	250.0	15.00	88.10	21635.0	0.01	-7.9	-1.06	0
Seawater	SW2	11/07/22	18.477778	121.412222	0.0045	0.00	-	-	-	-	-	105	0.10	1253.0	93.0	193.0	13.00	91.90	16415.0	0.01	-4.4	-0.28	0
Well	W1	11/08/22	18.453212	121.405746	4.9971	2.55	6.71	2,277	28.35	6.3767	1,403.33	233	8.26	16.4	433.0	343.0	18.80	24.50	653.0	1.93	-17.2	-3.04	0
Well	W2	11/08/22	18.395118	121.409731	3.5171	8.00	7.81	1,534	26.56	7.1000	978.67	318	67.24	537.0	86.4	40.6	15.20	15.70	258.0	0.01	-26.4	-5.03	0
Well	W3	11/07/22	18.411940	121.392220	3.8926	7.26	7.00	1,130	27.48	8.7867	723.67	276	76.63	193.0	663.0	46.6	7.87	0.25	184.0	0.01	-24.8	-3.93	0
Well	W4	11/08/22	18.433721	121.440850	13.7714	2.63	7.10	310	28.21	6.1600	201.33	88	1.80	38.5	14.4	32.8	0.45	59.10	16.0	0.01	-31	-4.98	0
Well	W5	11/08/22	18.441522	121.475235	5.6111	0.05	8.33	938	28.72	6.1533	600.33	158	135.49	279.0	14.4	39.4	19.60	76.40	102.0	0.01	-25.6	-4.71	0
Well	W6	11/08/22	18.444170	121.419720	1.5581	2.77	7.13	640	27.44	6.3856	327.00	239	6.53	84.5	64.4	44.5	9.55	0.55	39.0	0.01	-25.8	-4.85	0
Well	W7	11/08/22	18.440224	121.398581	13.6053	4.18	6.70	237	27.53	6.0700	154.33	70	1.82	31.0	13.7	25.8	0.68	20.30	16.0	0.01	-25.8	-4.79	0
Well	W8	11/08/22	18.384274	121.435556	7.1323	7.57	6.89	351	28.38	6.0633	228.00	120	3.40	30.7	146.0	40.9	0.05	20.00	7.8	0.01	-29.4	-5.56	0
Well	W9	11/08/22	18.394191	121.426934	10.2582	7.06	6.62	214	29.83	5.8900	139.33	50	2.45	36.2	15.6	34.2	0.05	16.70	12.0	0.01	-31.3	-5.86	0
Well	W10	11/09/22	18.305310	121.480800	12.5790	14.71	6.36	194	28.04	6.5500	125.67	41	1.42	32.5	15.2	22.2	0.26	7.32	8.8	0.01	-28.1	-5.12	0
Well	W11	11/09/22	18.355498	121.423004	12.5785	10.95	7.08	450	27.62	7.5900	289.67	180	2.80	35.0	421.0	43.0	0.40	47.40	17.0	0.01	-27	-4.89	0
Well	W12	11/08/22	18.399533	121.445003	15.6256	5.62	6.89	276	27.83	5.1067	180.33	79	3.34	34.1	16.5	30.3	0.05	48.20	13.0	0.01	-27.6	-4.83	0
Well	W13	11/08/22	18.427742	121.424828	7.1482	4.10	6.80	250	27.79	5.6767	161.00	96	2.36	25.0	31.6	32.6	0.42	29.70	7.8	0.01	-26.3	-4.9	0
Well	W14	11/09/22	18.131045	121.348885	45.199155	36.75	5.51	208	26.86	5.4667	131.67	4	2.64	1.0	17.8	27.1	1.11	11.00	7.8	0.01	-32.1	-5.46	0
Well	W15	11/08/22	18.292519	121.433765	18.296736	16.87	6.88	262	27.71	6.3500	170.00	89	1.46	33.0	77.2	37.3	0.05	26.90	0.2	0.01	-29.7	-5.05	0
Well	W16	11/09/22	18.199312	121.348508	40.87704	29.89	6.59	217	28.89	4.7467	141.00	63	2.32	24.8	77.2	33.0	0.05	9.52	0.2	0.60	-25.6	-4.86	0
Well	W17	11/09/22	18.214927	121.415163	73.1526	25.66	6.79	220	27.42	3.0833	141.00	62	4.55	35.0	120.0	27.5	0.74	6.04	11.0	0.37	-26.6	-4.88	0
Well	W18	11/08/22	18.409103	121.422114	9.5661	59.79	7.10	591	27.66	7.9033	378.00	170	33.05	61.5	29.3	44.3	4.46	30.80	43.0	0.36	-35.7	-5.93	0
					MDL									0.30	0.30	0.1	0.10	0.50	0.40	0.02			2

\*Symbols with a hyphen (-) mean no data were gathered or analyzed, whereas zero (0) means nothing is recorded.

\*MDL/2 was used to substitute data < MDL if the skewness is high, with a geometric standard deviation of >3, otherwise  $\frac{MDL}{\sqrt{2}}$  (Glass & Gray, 2001)

Table 3. Details of statistical data of different water quality parameters analyzed in wells

Parameter	Method	MDL*	Min	Max	Average	Standard Deviation
pH	Horiba multi-meter probe (Model U-50)	-	5.51	8.33	6.91	0.59
EC ( $\mu\text{S}/\text{cm}$ )	Horiba multi-meter probe (Model U-50)	-	194	2277	572	567
TDS ( $\text{mg}/\text{L}$ )	Horiba multi-meter probe (Model U-50)	-	125.67	1403.33	359.69	352.49
DO ( $\text{mg}/\text{L}$ )	Horiba multi-meter probe (Model U-50)	-	3.0833	8.7867	6.1533	1.2839
$\text{HCO}_3^-$ (ppm)	Hach digital titrator	-	4	318	130	89
**As ( $\mu\text{g}/\text{L}$ )	Digital Arsenator (Palintest)	2	< 2	< 2	1.41	0.00
$\text{NO}_3^-$ (ppm)	Digital Nitrate Meter	-	1.42	135.49	19.86	36.73
$\text{Na}^+$ (ppm)	3113 B. AAS Method	0.3	1.0	537.0	84.9	132.1
$\text{Ca}^{2+}$ (ppm)	3113 B. AAS Method	0.3	13.7	663.0	125.4	185.4
$\text{Mg}^{2+}$ (ppm)	3113 B. AAS Method	0.1	22.20	343.00	52.51	72.8
$\text{K}^+$ (ppm)	3113 B. AAS Method	0.1	0.05	19.60	4.43	6.82
$\text{SO}_4^{2-}$ (ppm)	4500 $\text{SO}_4^{2-}$ E. Method	0.5	0.25	76.40	25.02	20.90
$\text{Cl}^-$ (ppm)	4500 $\text{Cl}^-$ B. Method	0.4	0.20	653.00	77.59	159.73
$\text{Br}^-$ (ppm)	4500 $\text{Cl}^-$ G. Method	0.02	0.01	1.93	0.19	0.47

\*MDL for trace elements only; \*\*For As, all measured concentrations were below MDL (2  $\mu\text{g}/\text{L}$ ). To allow for descriptive analysis. To allow for descriptive statistical analysis without the bias of zero substitution, non-detect values were replaced with  $\frac{\text{MDL}}{\sqrt{2}}$  (Glass & Gray, 2001)

Arsenic (As) concentrations across all samples revealed that ARB remain below MDL (< 2  $\mu\text{g}/\text{L}$ ). This is well below the PNSDW (2017) guideline value of 10  $\mu\text{g}/\text{L}$ . The absence of geogenic As is a significant finding, as it suggests that the alluvial aquifers are currently under oxidizing conditions, with pH values ranging from acidic to near-neutral, typical of many natural environments. This is why most of the wells are unaffected by As enrichment. The rest of the samples are substantially low because As concentrations in open seawater and river water are typically 1.5  $\mu\text{g}/\text{L}$  and 0.1–8  $\mu\text{g}/\text{L}$ , respectively (Smedley & Kinniburgh, 2002).

The abundance of cations in all groundwater samples showed the following trend:  $\text{Ca}^{2+} > \text{Na}^+ > \text{Mg}^{2+} > \text{K}^+$ , while the variation of anions was observed as follows:  $\text{HCO}_3^- > \text{Cl}^- > \text{SO}_4^{2-} > \text{NO}_3^- > \text{Br}^-$ . The distribution of ions in the basin reveals a clear transition from mineral-weathering dominance inland to marine influence near the coast. The dominance of  $\text{Ca}^{2+}$  and  $\text{HCO}_3^-$  in most samples suggests carbonate weathering in the upstream reaches and accumulation as water flows down the alluvial plain, while a significant increase in  $\text{Na}^+$  and  $\text{Cl}^-$

concentrations is observed in samples close to the coastline. Twelve of 18 well samples are coming from freshwater with EC less than 500  $\mu\text{S}/\text{cm}$ , primarily found in upstream sections, four are under marginal water with EC from 500 to 1500  $\mu\text{S}/\text{cm}$ , and the remaining two near the coast have an EC value greater than 1500  $\mu\text{S}/\text{cm}$  which suggests possible saltwater contamination (Davis & De Wiest, 1966). The degree of salinization at these two sites is indicated by an increase in TDS, which is also observed with an increase in cations and anions. Since most of the well samples are dominated by  $\text{HCO}_3^-$ ,  $\text{Cl}^-$ , and  $\text{SO}_4^{2-}$ , they can generally be classified as freshwater. However, few samples showed dominance in EC, TDS,  $\text{Cl}^-$ , and  $\text{Na}^+$  levels, including river samples B2 and B3 and well samples W2 and W5. The cause, however, should be examined.

#### 4.2. Correlation of physicochemical parameters of samples

The correlation matrix of various hydrochemical parameters, as shown in Table 4, indicates that EC and TDS are strongly correlated with  $\text{Na}^+$ ,  $\text{Ca}^{2+}$ ,  $\text{Mg}^{2+}$ ,  $\text{K}^+$ , and  $\text{Cl}^-$ , while moderately correlated with  $\text{SO}_4^{2-}$ . The

same correlation was observed by Yadav et al. (2018) and affirms that these ions are major contributors to water salinity and ionic strength. Major cations such as  $\text{Na}^+$ ,  $\text{Ca}^{2+}$ ,  $\text{Mg}^{2+}$ , and  $\text{K}^+$  are strongly correlated with  $\text{Cl}^-$ , suggesting a common origin for these ions.

Table 4. Correlation matrix of different water quality parameters

Param.	pH	EC	TDS	DO	$\text{HCO}_3^-$	$\text{NO}_3^-$	$\text{Na}^+$	$\text{Ca}^{2+}$	$\text{Mg}^{2+}$	$\text{K}^+$	$\text{SO}_4^{2-}$	$\text{Cl}^-$	$\text{Br}^-$
pH	<b>1.00</b>												
EC	0.30	<b>1.00</b>											
TDS	0.34	<b>0.97</b>	<b>1.00</b>										
DO	0.18	-0.28	-0.34	<b>1.00</b>									
$\text{HCO}_3^-$	0.16	0.12	0.01	0.07	<b>1.00</b>								
$\text{NO}_3^-$	<b>0.41</b>	-0.09	-0.16	0.12	0.46	<b>1.00</b>							
$\text{Na}^+$	0.37	<b>0.83</b>	<b>0.72</b>	-0.06	0.17	0.11	<b>1.00</b>						
$\text{Ca}^{2+}$	0.30	<b>0.71</b>	<b>0.73</b>	-0.16	0.11	-0.14	0.46	<b>1.00</b>					
$\text{Mg}^{2+}$	0.25	<b>0.93</b>	<b>0.91</b>	-0.32	0.16	-0.17	<b>0.62</b>	<b>0.71</b>	<b>1.00</b>				
$\text{K}^+$	0.35	<b>0.98</b>	<b>1.00</b>	-0.34	0.03	-0.12	<b>0.72</b>	<b>0.73</b>	<b>0.91</b>	<b>1.00</b>			
$\text{SO}_4^{2-}$	0.12	<b>0.68</b>	<b>0.59</b>	-0.16	0.04	0.08	<b>0.77</b>	0.28	<b>0.53</b>	<b>0.60</b>	<b>1.00</b>		
$\text{Cl}^-$	0.33	<b>0.96</b>	<b>0.99</b>	-0.34	-0.01	-0.16	<b>0.73</b>	<b>0.72</b>	<b>0.90</b>	<b>0.98</b>	<b>0.58</b>	<b>1.00</b>	
$\text{Br}^-$	-0.27	0.12	-0.06	0.23	0.17	-0.06	0.25	<b>-0.02</b>	0.24	-0.05	0.27	-0.07	<b>1.00</b>

\*Parameters showing  $r > 0.7$  are considered as strongly correlated, whereas  $r$  between 0.5 and 0.7 shows moderate correlation (Maurya et al., 2019)

### 4.3. IDW Spatial Distribution

The spatial variation of TDS (directly related to EC), chloride, sodium, and sulfate, as shown in Fig. 4, demonstrates the coincidence of high concentrations across the study area. This is because regions with high TDS (or EC) are primarily responsible for the high concentrations of sodium and chloride resulting from water salinity. The analysis shows similarities in the variations of chloride, a minor anion, and sodium, a major cation, which are primarily responsible for water salinity.

### 4.4. Variation of isotopic composition of samples

#### 4.4.1. Establishing the Local Meteoric Water Line (LMWL)

There is an average of 3,158 mm of rain per year from 2019 to 2023 (Fig. 5). Historical data indicate the rainy season is from August to February, while the dry season lasts in the remaining months of the year. Over the last five years, the peak rainfall is typically in November; therefore, isotope sampling was conducted in November, while the least rainfall is typically in April.

The depth of rainwater recorded monthly using the improvised rainwater collector (IRC) and RS1 rain sampler versus the AWS Rain Gauge every month was graphed (Fig. 6). The percent difference ranged from 0.69% to 24.18%, with an average of 9.89%, which indicates that the method used of collecting rainwater samples was acceptable.

The Abulug LMWL was determined using scatter plot of delta Oxygen-18 ( $\delta^{18}\text{O}$ ) versus delta Hydrogen-2 ( $\delta^2\text{H}$ ) values, expressed in per mil (‰) units, of all rainwater samples (Fig. 7). The LMWL of Abulug area is about  $\delta^2\text{H} = 8.71 \delta^{18}\text{O} + 16.375$  which coincides with both the Philippine Meteoric Water Line (PMWL) and the Global Meteoric Water Line (GMWL) which are about  $\delta^2\text{H} = 8 \delta^{18}\text{O} + 12$  (Gerardo-Abaya, 2005) and  $\delta^2\text{H} = 8 \delta^{18}\text{O} + 10$  (Craig, 1961) respectively. The LMWL showed a slight evaporative enrichment of heavy isotopes, as indicated by the measured slope and intercept shown in the figure. Local meteorological conditions in ARB may lead to deviations from the global and national averages.

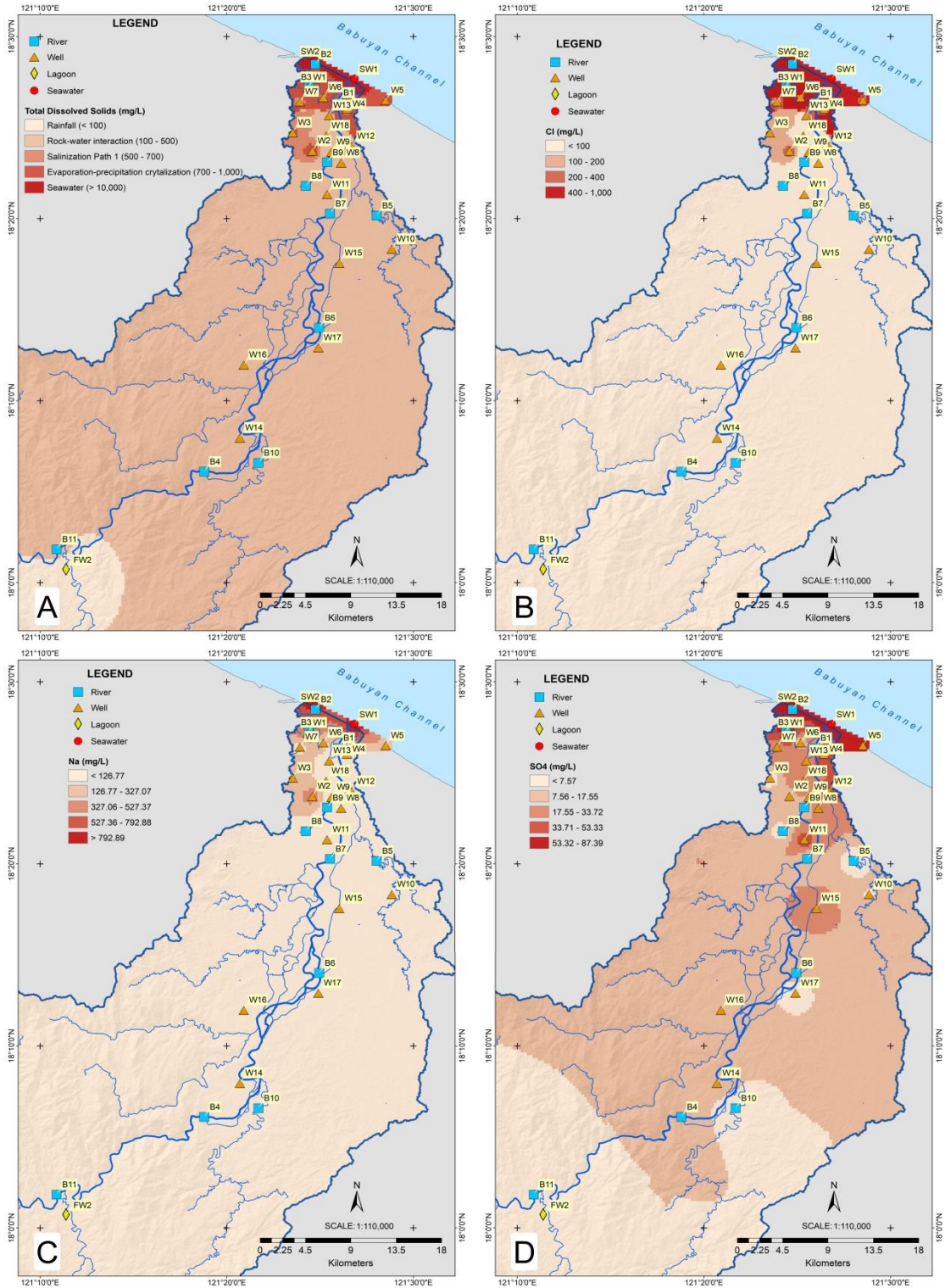


Figure 4. Spatial variation of water quality parameters (A) TDS, (B) chloride, (C) sodium, and (D) sulfate

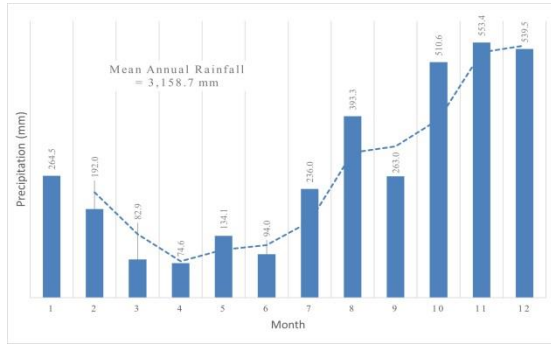


Figure 5. Mean monthly rainfall at NCES, Abulug, from 2019 to 2023

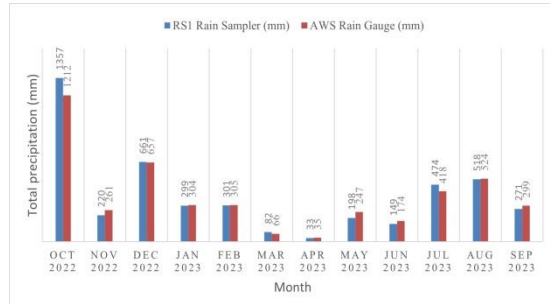


Figure 6. Comparison of monthly precipitation measured using RS1 Rain Sampler vs. AWS Rain Gauge

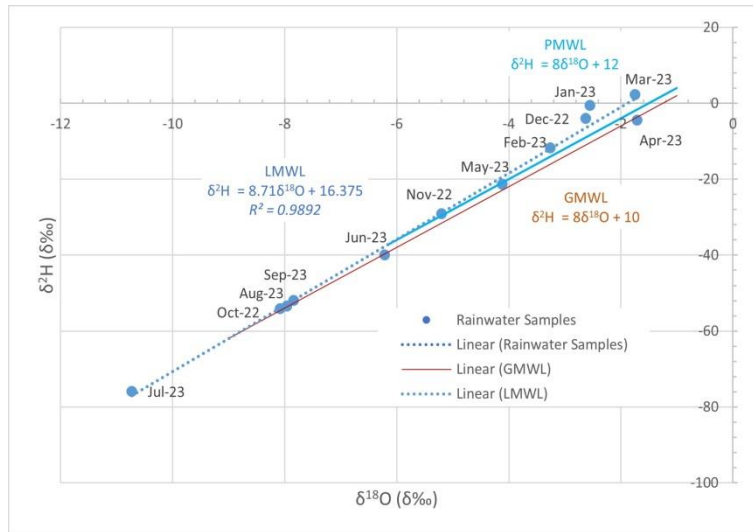


Figure 7.  $\delta^{18}\text{O}$  versus  $\delta^2\text{H}$  diagram of the rainwater samples gathered from October 2022 to September 2023 as compared to PMWL and GMWL

The amount of rainfall collected in Abulug from October 2022 to January 2023 ranged from 400 mm to 1200 mm, with the highest recorded in October 2022, during the severe tropical storm Nalgae (locally named Paeng), which brought heavy rains and floods to northern Luzon. Prolonged dry weather hit Abulug from January to July 2023. This was comparable to the historical monthly rainfall recorded by AWS in the same area. The collection of rainwater samples during the pre-monsoon period is between December 2022 and May 2023. These samples showed higher isotope enrichment than rainwater samples during the monsoon onset, from June

to November. The behavior could be explained by a change in the Philippines' predominant wind systems: the Northeast (NE) monsoon, which typically lasts from November to February, and the Southwest (SW) monsoon, which typically lasts from July to September. Gerardo-Abaya (2005) reported similar behavior in isotope data from rainwater samples collected at different locations in the Philippines.

#### 4.4.2. Isotope analysis of samples

As indicated in Fig. 8, there is a gradual depletion in heavy isotopes, both  $\delta^2\text{H}$  and  $\delta^{18}\text{O}$ , as the water moves inland from the

coast. This is because heavier isotopes are left behind when lighter isotopes generally

evaporate and are easily absorbed into precipitation.

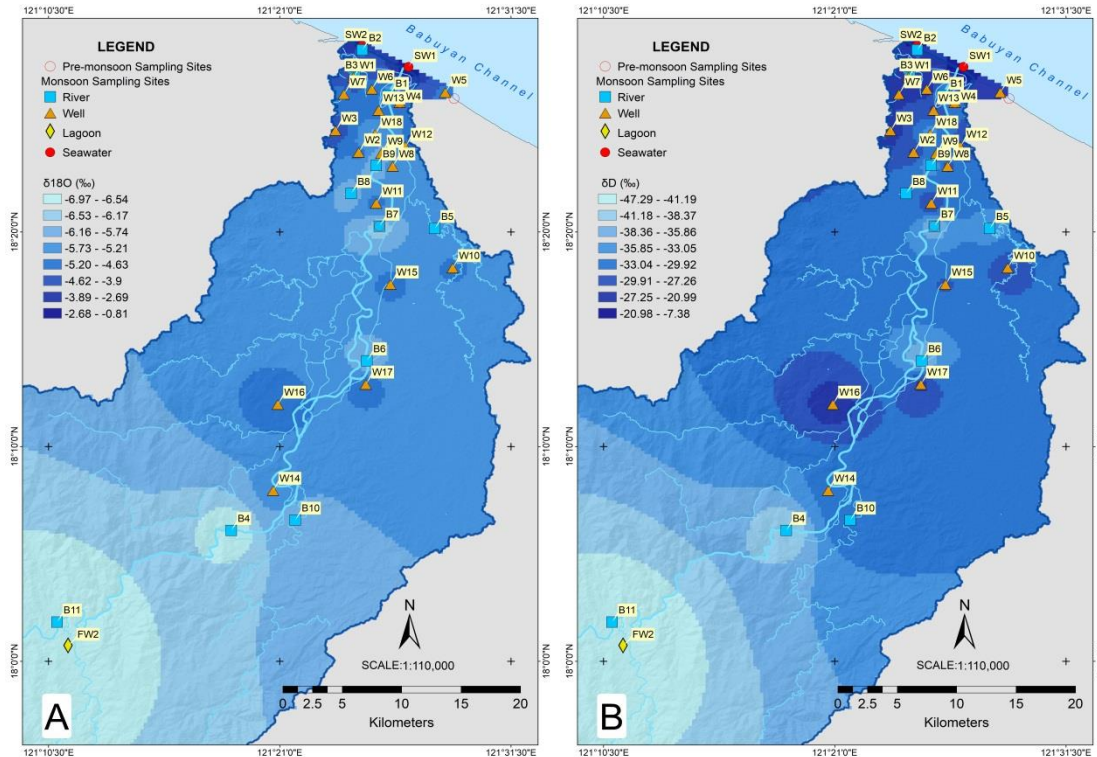


Figure 8. Geographical variation in levels of (A)  $\delta^2\text{H}$  and (B)  $\delta^{18}\text{O}$  of samples in the Northern Abulug River Basin

The isotopic data of groundwater, seawater, and freshwater in ARB were also plotted along with the LMWL (Fig. 9). During the monsoon, the  $\delta^{18}\text{O}$  composition of the well samples ranged from  $-5.93\text{‰}$  to  $-3.04\text{‰}$ , with an average of  $-4.93\text{‰}$ , while  $\delta^2\text{H}$  composition ranged from  $-35.7\text{‰}$  to  $-17.2\text{‰}$ , with an average of  $-27.24\text{‰}$ . For the river water samples,  $\delta^{18}\text{O}$  composition ranged from  $-6.97\text{‰}$  to  $-5.67\text{‰}$ , with an average of  $-6.25\text{‰}$ , whereas  $\delta^2\text{H}$  composition ranged from  $-42.20\text{‰}$  to  $-30.40\text{‰}$ , with an average of  $-36.97\text{‰}$ .

Although samples during pre-monsoon were limited to five, the DPWH discharge records confirm that these samples were collected during stable baseflow conditions, with average  $Q = 75.85 \text{ m}^3/\text{s}$  (Fig. 10a). A

salinity peak was observed in W1 ( $2770 \mu\text{S}/\text{cm}$ ), suggesting a conservative baseline for saltwater intrusion during the lowest river flow. On the other hand, during the monsoon, the massive freshwater discharge ( $Q = 502.8 \text{ m}^3/\text{s}$ ) pushes the salt wedge back, thereby reducing the salinity of the samples. By aligning sampling times with the OSU-TPX08 tide (Fig. 10b), the slightly higher tidal stage during the monsoon event would typically favor saline intrusion. However, EC decreased to  $2277 \mu\text{S}/\text{cm}$ , suggesting that the massive river flow is the dominant force, acting as a hydraulic barrier that pushes the salt wedge farther out to sea and freshens the groundwater near the coast. Although EC decreased at W1 during the monsoon period, the values remain indicative of moderately saline groundwater. While a

quantitative mixing ratio cannot be determined from the available data, the EC reduction indicates incomplete flushing, suggesting that residual salinity from a prior intrusion persists even during the monsoon period.

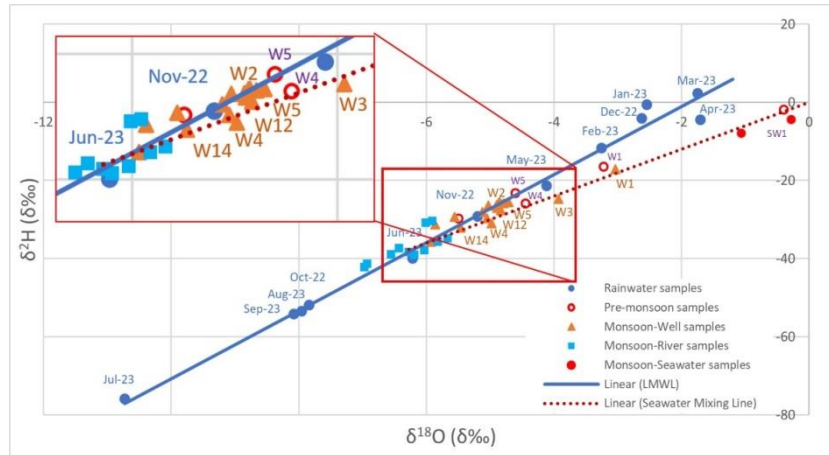


Figure 9. Hydrological and tidal context of the sampling period. (A) long-term mean monthly average ( $\text{m}^3/\text{s}$ ) (Data source: DPWH, 2004–2016) at Lucban Bridge, Abulug, and (B) predicted tidal height (masl) during the sampling dates derived from OSU TPX08, for ARB. Red and orange represent sampling windows conducted during pre-monsoon and monsoon periods, respectively. Markers indicate specific timing sampling relative to the semi-diurnal tidal cycle

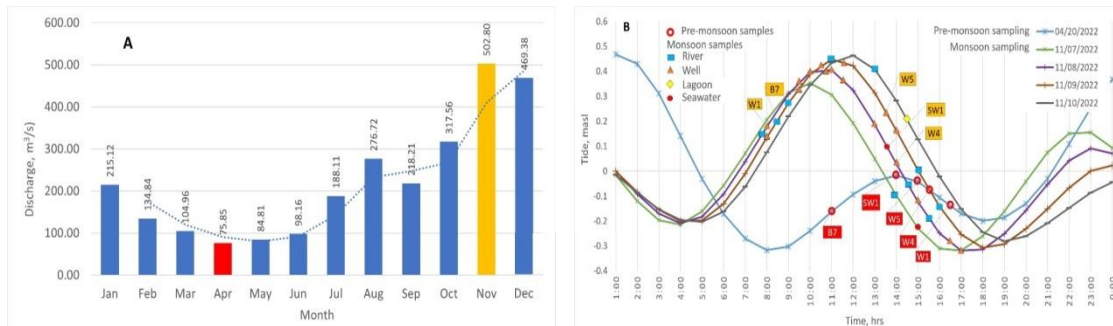


Figure 10.  $\delta^{18}\text{O}$  versus  $\delta^{2}\text{H}$  distribution of the samples gathered on pre-monsoon (April 20, 2022) and during monsoon (November 7–10, 2022)

The isotopic signatures show consistent depletion of isotopes across the five sample sites from the pre-monsoon to the monsoon period. For example, in the river sample B7, the  $\delta^{18}\text{O}$  signature shifted from  $-5.49\text{‰}$  to  $-6.55\text{‰}$ . The shift corresponds to the transition from low-flow baseflow to high-flow runoff, which introduces isotopically lighter precipitation into the system. Furthermore, the depletion in seawater, SW1,

from  $-0.39\text{‰}$  to  $-1.06\text{‰}$  suggests that the increase in river momentum during the monsoon competes with tidal forcing. This leads to a greater freshwater fraction even at marine sampling points, highlighting the importance of using these isotopic values as a baseline for future seasonal salt-wedge modeling. The depletion in wells W4 and W5 is responding to monsoon rainfall recharge, which is isotopically lighter than the

evaporated pre-monsoon groundwater. W1 remained isotopically stable, with only a +0.18‰ shift, suggesting a deeper or larger groundwater source.

The LMWL, described by the equation  $\delta^2\text{H} = 8.71 \delta^{18}\text{O} + 16.375$  is shown as a reference. The stable isotope data indicate that the groundwater is mainly of precipitation origin and is affected by varying degrees of evaporative enrichment of its isotopic composition. Normally, surface water is more enriched in heavier isotopes than groundwater because surface water bodies are more susceptible to evaporation than groundwater, especially in arid or semi-arid regions. But the case with ARB is the opposite.

The precipitation in June apparently mainly contributes to runoff rather than to groundwater recharge. This is illustrated in the figure, where river samples mostly fall within the LMW regression line for June. During the dry season, specifically from February to July, this June precipitation infiltrates into the unconfined aquifer as groundwater. However, due to the elevated hydraulic pressure, this water leaches out and becomes river water. This phenomenon is observed particularly in losing streams, where rainfall, particularly

during dry months, serves as the primary water source.

On the other hand, well samples fall within the November zone. This denotes that rain has recharged these groundwater samples. Figure 9 further shows that rainfall during the dry season does not contribute to groundwater recharge, as it comes from shallow aquifers. Thus, these observations prove that rainfall during the wet periods from August to January effectively contributes to groundwater recharge. However, few samples fall within the mixing line, indicating possible mixing between coastal groundwater and seawater.

#### 4.5. Geochemical evolution of groundwater

Numerous diagrams are used in different research literatures on water chemistry to illustrate primary hydrochemical water types and emphasize the dominant geochemical processes that influence groundwater composition. This study applied two of the most recognized diagrams, the Piper and Chadha diagrams, in conjunction with ionic ratios and the  $\delta^{18}\text{O}$  vs.  $\delta\text{D}$  diagram. Three different groups of samples were identified and summarized in Table 5.

Table 5. Classification of the samples based on the piper diagram

Group	Chemical facies	Chemical formula	No. of samples	%
1	Calcium Magnesium Sulphate	$\text{CaMgSO}_4$	5	15.6
2	Calcium Magnesium Bicarbonate	$\text{CaMgHCO}_3$	21	65.6
3	Sodium Chloride	$\text{NaCl}$	6	18.8

Five of 32 samples belong to Group 1, the Ca-Mg-SO<sub>4</sub> water type: W14, W1, W3, W12, and W4. These samples fall within the Reverse Ion Exchange field of Chadha's diagram. In addition, 21 samples belong to Group 2 or the Ca-Mg-HCO<sub>3</sub> water type. Groundwater samples from this type have pH, total alkalinity, and ion concentrations similar to those of nearby rivers. In fact, the river water samples fall within the Recharge Water category on Chadha's diagram, confirming that these rivers are the source of recharge for

wells. Despite the observation of a variety of hydrochemical facies, CaHCO<sub>3</sub> is dominant. While Group 3 consists of six samples - SW2, SW1, B2, B3, W5, and W2, which belong to the Na-Cl water type of the Piper diagram and belong within the saltwater of Chadha's diagram. These samples fall under the 7<sup>th</sup> sub-field of Chadha's diagram: alkali metals exceed alkaline earths, and strong acidic anions exceed weak acidic anions, which generally create alkalinity problems (Maurya et al., 2019).



In samples where the origin of salinity is not clear, using a single measure, especially in coastal regions, bromide concentration and stable isotope values are major discriminators (Benaafi et al., 2022; Du et al., 2015). As indicated in Table 6, the W1 hydrochemical and isotopic evidence is consistent with seawater mixing as indicated by elevated bromide concentration, enriched stable isotopes, reverse ion exchange category, and relatively closer to seawater  $\text{Cl}^-/\text{Br}^-$  molar ratio of  $655 \pm 4$  (Custodio E & Herrera C, 2000; Nosair et al., 2025), suggesting saltwater intrusion. For seawater,  $\text{Cl}^-$  and  $\text{Br}^-$  increase together, but in the case of W3,  $\text{Br}^-$  is almost absent. This means that  $\text{Cl}^-$  is coming from another source. Its hydrochemical characteristics are consistent with groundwater composition controlled by rock-water interaction through silicate weathering of

feldspars. This is evidenced by the dominance of  $\text{CaMgSO}_4$  facies and the presence of reverse cation exchange. These observations, together with the sample's position in Gibb's diagram within the weathering dominance field, support the idea that W3 is largely governed by rock-water interaction rather than seawater interaction. On the other hand, W2 and W5, although classified as NaCl facies, exhibit elevated chloride concentration coupled with extremely low bromide levels which result in a very high  $\text{Cl}^-/\text{Br}^-$  ratio  $>10,000$ , significantly deviating from the seawater signature, suggesting rock-water interaction, with possible major contribution from halite dissolution (Cartwright et al., 2004; Kloppmann et al., 2001). These interpretations represent a geochemical inference and remain a hypothesis to be tested by future hydraulic and geophysical investigations.

Table 6. Hydrochemical and isotopic indicators of groundwater salinization in processes in selected wells

Sample	Chemical facies	$\text{Cl}^-$ (ppm)	$\text{Br}^-$ (ppm)	$\text{Cl}^-/\text{Br}^-$ ratio	$\delta^2\text{H}$ (‰)	$\delta^{18}\text{O}$ (‰)
W1	$\text{CaMgSO}_4$ / Reverse ion exchange	653.0	1.93	338.3	-17.2	-3.04
W3	$\text{CaMgSO}_4$ / Reverse ion exchange	258.0	0.01	25,800.0	-24.8	-3.93
W2	NaCl/ Saltwater	184.0	0.01	18,400.0	-26.4	-5.03
W5	NaCl/ Saltwater	102.0	0.01	10,200.0	-25.6	-4.71

#### 4.6. Salinization of Groundwater

The Gibb's plot of  $\log \text{TDS}$  versus  $\text{Na}^+(\text{Na}^+ + \text{Ca}^{2+})$  and  $\log \text{TDS}$  versus  $\text{Cl}^-/(\text{Cl}^- + \text{HCO}_3^-)$ , as shown in Fig. 12a and 12b, respectively, further indicate that weathering due to rock dominance with  $30 < \text{TDS} < 1000$ , and salinization due to evaporation-precipitation crystallization dominance with  $\text{TDS} \geq 1000$ , are significantly influencing the groundwater's chemistry as a result of the climatic and geographic condition. Most groundwater samples fall under the weathering category, indicating that rock-water interaction has a significant impact on the region's groundwater chemistry. The general geology provides information on the silicate weathering sequence of the basin, from upstream to downstream. As water

moves from the high-relief rocks such as diorite, granodiorite, and dacite down to the alluvial plain, it undergoes a series of predictable chemical changes that enrich the Ca-Mg- $\text{HCO}_3$  signatures of the samples. As slightly acidic rainwater aggressively attacks the Ca-rich minerals of upstream rocks (e.g., Plagioclase Feldspars), it generates  $\text{HCO}_3^-$  and releases  $\text{Ca}^{2+}$  into the water (Wallmann et al., 2023). Even more reactive than the crystalline diorites are andesite/basalt and tuffaceous sediments found midstream. Basaltic rocks are rich in  $\text{Mg}^{2+}$ , while tuffaceous sediments have a high surface area and dissolve readily (Tang, 2021). By the time it reaches the alluvium sink, it carries the chemistry of everything it passed through and acts as a "blender" of all upstream rock types. This confirms Chadha's diagram, reiterating that upstream river water

recharges these wells. The same results were found in Leyte (Asio & Jahn, 2007), identifying rock weathering of basaltic rock formations as the major source of cation enrichment in stream water. In contrast to some peat rivers in Southeast Asia, such as those in Borneo (Ukotije-Ikwut et al., 2023), the upstream of ARB remains more mineral-rich, attributed to the active tectonic and volcanic geology of Northern Luzon. It is also apparent that well samples, W2 and W5, and river samples, B2 and B3, near the coast, undergo salinization with  $\text{Na}^+(\text{Na}^+ + \text{Ca}^{2+})$

value of 0.8 and  $\text{TDS} > 700$  ppm. The Piper diagram makes it clear that these two wells lie within Salinization Path 1, where mixing of  $\text{Na-HCO}_3$  and  $\text{Na-Cl}$  waters occurs. Liu et al. (2009) conducted studies on 21 major rivers in Luzon, Philippines, including those adjacent to the ARB, and found that the weathering of basaltic and andesitic rocks from the Cordillera Mountains leads to a predictable leaching sequence of  $\text{Ca} > \text{Na} > \text{Mg} > \text{Si}$ . The ARB behaves similarly due to the island's shared volcanic-sedimentary rock composition.

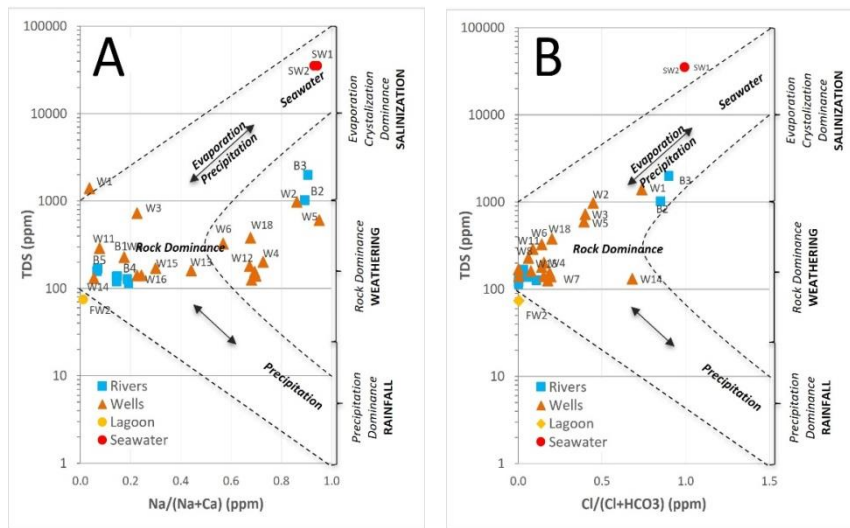


Figure 12. Scatter plot (A)  $\text{Na}^+(\text{Na}^+ + \text{Ca}^{2+})$  and TDS; (B)  $\text{Cl}^-(\text{Cl}^- + \text{HCO}_3^-)$  and TDS

On the other hand, it is worth noting that W1 is influenced by seawater intrusion, as evidenced by  $\delta^{18}\text{O}$  vs.  $\delta^2\text{H}$ , indicating mixing between meteoric water and seawater, with hydrogeochemical processes characterized by weathering and reverse ion exchange, as revealed by Gibb's and Chadha's diagrams. This phenomenon is typical in aquifers of transitional salinity, which occurs when seawater intrudes into freshwater. Similarly, the coastal aquifer of Korba, Tunisia, shows reverse ion exchange triggered by marine intrusion (Ayari et al., 2023). Well samples W4, W12, and W14, with the category

reversed ion exchange in Piper and Chadha's diagram, are controlled by rock-water interaction, unlike most other samples. This occurs in areas where the predominant rock types such as gypsum, limestone, or salt-bearing formations release dissolved ions like calcium, magnesium, sodium, and sulfate into the groundwater, which contribute salts through weathering processes. In almost all groundwater samples, ion concentrations are increased by weathering and, to a lesser extent, by salinization (Maurya et al., 2019). These plots confirm the results of using both Piper's and Chadha's Diagrams.

**4.7. Simpson ionic ratio to infer saltwater contamination**

The impact of seawater intrusion on groundwater chemistry and the discovery of various hydrochemical processes affecting water quality have both been enabled by ionic chemical ratios (El Moujabber et al., 2006; Ezzeldin, 2022) and geological information of the study area (Gurmessa et al., 2022). The geographical variation in the samples' Simpson ratios was mapped superimposed on the basin's geological map, as shown in Fig. 13.

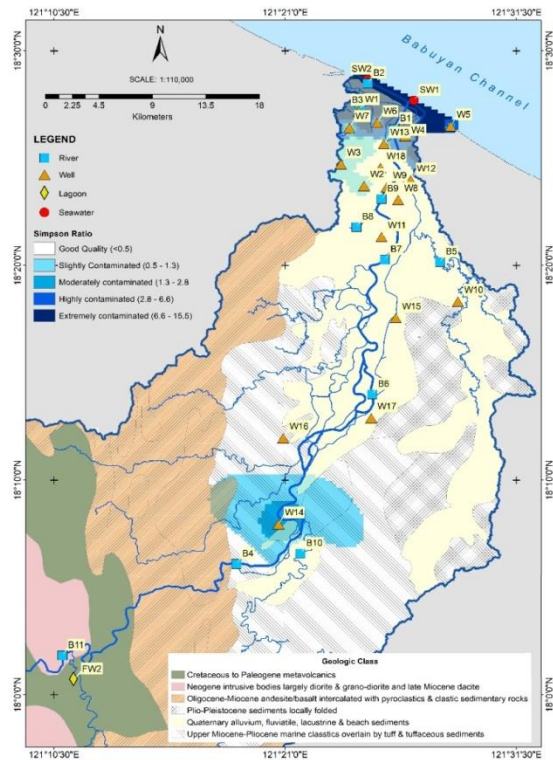


Figure 13. Simpson ionic ratio ( $Cl/HCO_3$ ) results with respect to their data location. A  $Cl/HCO_3 > 0.5$  (pink to red) implies salinization due to seawater mixing with groundwater and river water

El Moujabber et al. (2006) divided  $Cl/(HCO_3 + CO_3)$  values into five classes, and samples were classified as indicated in Table 7. 5 of 18 wells, or 28%, are saline-contaminated, with Simpson ratios  $> 0.5$ . The Simpson ratio  $> 0.5$  data with a location relatively far from

the Babuyan Channel may indicate other sources of salinity besides seawater intrusion (e.g., brine-fossil water). The same source of salinity was found by Tan et al. (2020) in a sample approximately 40 m from the coastline, with a Simpson ionic ratio  $< 0.5$ .

Table 7. Classification of groundwater salinity based on Simpson ionic ratio values

Simpson ionic ratio	Class	Samples	Distance from coast (km)
0.5–1.3	Slightly contaminated	W2	8.00
		W3	7.26
		W5	0.05
1.3–2.8	Moderately contaminated	W1	2.55
		W14	36.75
2.8–6.6	Highly contaminated	B2	0.14
6.6–15.5	Extremely contaminated	B3	2.45
		SW1	0.00
		SW2	0.00

W14 is composed of marine clastics from the Upper Miocene-Pliocene, which originated from a marine environment called paleosaline groundwater. These marine clastics may contain residual salts from the original marine depositional environment, which were overlain by tuff and tuffaceous sediments of volcanic origin. Salts can be released during the weathering process of both volcanic and marine clastic deposits.

**4.9. Conceptual Model of Groundwater Salinization**

The conceptual cross-section (Fig. 14) synthesizes the hydrochemical and isotopic evidence. It highlights the coexistence of multiple salinization processes in the ARB, including seawater intrusion in the coastal zone, transitional hydrochemical processes controlled by rock-water interaction occurring inland, and residual salinity from paleo-saline groundwater influencing the upstream. This integrated representation provides a framework for understanding the evolution and possible spatial variability of groundwater salinity in the basin.

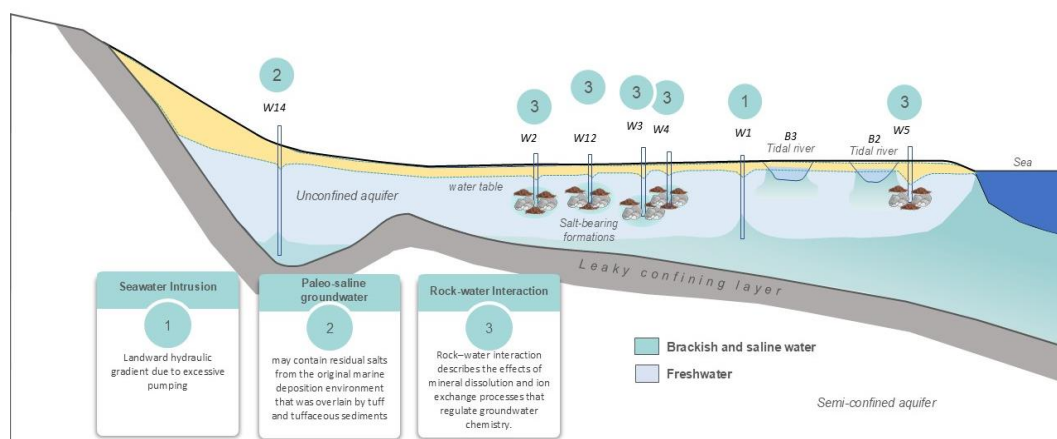


Figure 14. Conceptual hydrogeological cross-section of the study area showing inferred salinization processes, freshwater-saltwater interface, and possible salinization processes. The position of salt-affected sampling wells is relative. The diagram is schematic and based on regional hydrogeological characteristics and geochemical interpretation

#### 4.10. Management and Policy Implications

The detection of reverse ion exchange in ARB indicates an active seawater front. In samples where direct SWI and the intrusion front along its transect should be designated as the sentinel well network, an immediate mortarium must be implemented to prevent early-stage encroachment from becoming irreversible. The conduct of geophysical assessments, such as Electrical Resistivity Tomography (ERT) and Transient Electromagnetic (TEM) surveys, across the ARB coastal interface, however, is recommended to map and provide a volumetric understanding of the saline wedge, which currently remains hidden beneath the signatures in geochemical diagrams. On the other hand, in wells where salinity is caused by rock-water interaction, including cation exchange, and by paleo-saline groundwater, controlled abstraction with an established dedicated monitoring network across the basin is commendable.

#### 5. Conclusions

The dearth of information in hydrogeological studies often constrains

research and development initiatives. However, the use of widely accepted methods remains useful for providing baseline datasets and initial understanding that can serve as a guideline for future research and development and policy recommendations. This study highlighted the various processes and mechanisms that impact groundwater salinization in the coastal region of the Abulug River Basin, using hydrochemical analysis and isotope tracing. Results revealed that while almost all the groundwater samples are mainly of precipitation origin, it also suggested that a complex salinization process is taking place in the study area, which results in three causes with distinguished salinity and isotopic signatures: SWI (W1-Santo Tomas, Abulug), brine fossil water or paleo-saline groundwater (W14-Mataguasi, Pudtul), and rock-water interaction such as cation exchange (W4-Alinunu, Abulug and W12-Banguian, Abulug), silicate weathering (W3-Curva, Pamplona), and halite dissolution (W2-Canayun, Abulug and W5-Bagu, Abulug). It is worth noting that salinity in W1 is caused by SWI, contrary to the local beliefs of tidal flooding. The generated hydrochemical variation reveals a clear

salinity gradient extending up to 8 km downstream. The Simpson ionic ratio indicates that the coastal aquifer is currently in a state of moderate encroachment, and the single upstream sampling site located 36.75 km from the coast suggests the presence of paleosoline groundwater trapped within the deeper units of ARB.

While extent and cause were determined, spatial interpolation is limited only to the designed sampling density. The results also do not reflect the basin's long-term trends or dynamics, as temporal variation in isotopic and chemical composition across different seasons remains unexamined. The detection of paleo-saline groundwater highlights the need for deeper exploratory drilling and a higher-density grid in the upstream sections. Even within a limited timeframe, stable isotopic signatures serve as robust fingerprints of water origin. Hence, the results can be applied to improve our understanding of the many hydrogeological mechanisms responsible for the salinization-induced degradation of groundwater. Local government agencies, in coordination with water resource authorities, should restrict groundwater extraction in identified hot spots and establish a network-based monitoring system or at least regular sampling. Nevertheless, the findings call for a more comprehensive exploration of coastal hydrologic processes in ARB and related factors affecting adjacent communities. This underscores the significance of government-level intervention in catalyzing frameworks that support and address salinization-induced groundwater quality issues.

### Acknowledgments

The authors are thankful to the Department of Science and Technology for funding this research and to the Isabela State University-Smart Water and Infrastructure Management R&D Center (ISU-SWIM) for providing financial support for the research. The authors also acknowledge the technical assistance of

Messrs. Raymond Sugang and Norman Mendoza of the Philippine Nuclear Research Institute, Philippines, for their support in isotopic analysis and for lending materials for the fieldwork.

### References

- Allen D.M., Suchy M., 2001. Geochemical evolution of groundwater on Saturna Island, British Columbia. *Canadian Journal of Earth Sciences*, 38(7), 1059–1080. <https://doi.org/10.1139/e01-007>.
- Anders R., Mendez G.O., Futa K., Danskin W.R., 2014. A geochemical approach to determine sources and movement of saline groundwater in a coastal aquifer. *Groundwater*, 52(5), 756–768. <https://doi.org/10.1111/gwat.12108>.
- American Public Health Association (APHA), 2017. *Standard Methods for the Examination of Water and Wastewater* (23<sup>rd</sup> ed). Washington DC: American Public Health Association.
- Asio V.B., Jahn R., 2007. Weathering of Basaltic Rock and Clay Mineral Formation in Leyte, Philippines. *Philippine Agricultural Scientist*, 90(3), 222–230.
- Ayari J., Ouelhazi H., Charef A., Barhoumi A., 2023. Delineation of seawater intrusion and groundwater quality assessment in coastal aquifers: The Korba coastal aquifer (Northeastern Tunisia). *Marine Pollution Bulletin*, 188, 114643. <https://doi.org/10.1016/j.marpolbul.2023.114643>.
- Ayers R.S., Westcot D.W., 1985. *Water quality for agriculture*. Rome: Food and agriculture organization of the United Nations, 29, 174.
- Benaafi M., Tawabini B., Abba S.I., Humphrey J.D., AL-Areeq A.M., Alhulaibi S.A., Usman A.G., Aljundi I.H., 2022. Integrated Hydrogeological, Hydrochemical, and Isotopic Assessment of Seawater Intrusion into Coastal Aquifers in Al-Qatif Area, Eastern Saudi Arabia. *Molecules*, 27(20), 6841. <https://doi.org/10.3390/molecules27206841>.
- Chadha D.K., 1999. A proposed new diagram for geochemical classification of natural waters and interpretation of chemical data. *Hydrogeology Journal*, 7(5), 431–439. <https://doi.org/10.1007/s100400050216>.
- Craig H., 1961. Isotopic Variations in Meteoric Waters. *Science*, 133(3465), 1702–1703. <https://doi.org/10.1126/science.133.3465.1702>.

- Department of Agriculture Bureau of Soils and Water Management (DA-BSWM), 2017. National Mapping, Characterization and Development of Spatial Database for the Coastal Areas Affected by Salinity. Accessed from <https://www.bswm.da.gov.ph/program/salinity/on> April 13, 2026.
- Du Y., Ma T., Chen L., Shan H., Xiao C., Lu Y., Liu C., Cai H., 2015. Genesis of salinized groundwater in Quaternary aquifer system of coastal plain, Laizhou Bay, China: Geochemical evidences, especially from bromine stable isotope. *Applied Geochemistry*, 59, 155–165. <https://doi.org/10.1016/j.apgeochem.2015.04.017>.
- El Moujabber M., Bou Samra B., Darwish T., Atallah T., 2006. Comparison of different indicators for groundwater contamination by seawater intrusion on the Lebanese coast. *Water Resources Management*, 20(2), 161–180. <https://doi.org/10.1007/s11269-006-7376-4>.
- Ezzeldin H.A., 2022. Delineation of Salinization and Recharge Sources Affecting Groundwater Quality Using Chemical and Isotopic Indices in the Northwest Coast, Egypt. *Sustainability (Switzerland)*, 14(24), 16923. <https://doi.org/10.3390/su142416923>.
- Gerardo-Abaya J., 2005. Determination of Recharge from Stable Isotope Data to the Hydrological Systems in the Southern Negros Geothermal Field and its Environs, Philippines. *Proceedings World Geothermal Congress*, 24–29.
- Gibbs R.J., 1970. Mechanisms controlling world water chemistry. *Science*, 170(3962), 1088–1090. Doi: 10.1126/science.170.3962.1088.
- Glass D.C., Gray C.N., 2001. Estimating Mean Exposures from Censored Data: Exposure to Benzene in the Australian Petroleum Industry. In *Ann. Occup. Hyg.*, 45(4), 275–282. <https://academic.oup.com/annweh/article/45/4/275/139056>.
- Gurmessa S.K., MacAllister D.J., White D., Ourdraog I., Lapworth D., MacDonald A., 2022. Assessing groundwater salinity across Africa. *Science of the Total Environment*, 828. <https://doi.org/10.1016/j.scitotenv.2022.154283>.
- Hajji S., Allouche N., Bouri S., Aljuaid A.M., Hachicha W., 2022. Assessment of seawater intrusion in coastal aquifers using multivariate statistical analyses and hydrochemical facies evolution-based model. *International Journal of Environmental Research and Public Health*, 19(1). <https://doi.org/10.3390/ijerph19010155>.
- International Atomic Energy Agency, 2007. Introduction to Water Sampling and Analysis for Isotope Hydrology. Non-serial Publications, IAEA.
- Kärnä T., Baptista A.M., Lopez J.E., Turner P.J., McNeil C., Sanford T.B., 2015. Numerical modeling of circulation in high-energy estuaries: A Columbia River estuary benchmark. *Ocean Modelling*, 88, 54–71. <https://doi.org/10.1016/j.ocemod.2015.01.001>.
- Klassen J., Allen D.M., Kirste D., 2014. Chemical indicators of saltwater intrusion for the Gulf Islands, British Columbia. Final Report, Department of Earth Sciences, Simon Fraser University. Accessed at [https://a100.gov.bc.ca/pub/acat/documents/r50327/ChemIndicatorsSWI\\_1462495790908\\_2492712699.pdf](https://a100.gov.bc.ca/pub/acat/documents/r50327/ChemIndicatorsSWI_1462495790908_2492712699.pdf) on April 13, 2026.
- Liu Z., Zhao Y., Colin C., Siringan F.P., Wu Q., 2009. Chemical weathering in Luzon, Philippines from clay mineralogy and major-element geochemistry of river sediments. *Applied Geochemistry*, 24(11), 2195–2205. <https://doi.org/10.1016/j.apgeochem.2009.09.025>.
- Maurya P., Kumari R., Mukherjee S., 2019. Hydrochemistry in integration with stable isotopes ( $\delta^{18}\text{O}$  and  $\delta\text{D}$ ) to assess seawater intrusion in coastal aquifers of Kachchh district, Gujarat, India. *Journal of Geochemical Exploration*, 196, 42–56. <https://doi.org/10.1016/j.gexplo.2018.09.013>.
- National Economic and Development Authority, 2026. Cagayan riverine zone development framework plan 2005–2030.
- Ohmer M., Liesch T., Goldscheider N., 2019. On the Optimal Spatial Design for Groundwater Level Monitoring Networks. *Water Resources Research*, 55(11), 9454–9473. <https://doi.org/10.1029/2019WR025728>.
- Philippine National Standards for Drinking Water, 2017. <https://www.fda.gov.ph/wp-content/uploads/2021/08/Administrative-Order-No.-2017-0010.pdf>.

- Prusty P., Farooq S.H., 2020. Seawater intrusion in the coastal aquifers of India - A review. *HydroResearch*, 3, 61–74. <https://doi.org/10.1016/j.hydres.2020.06.001>.
- Racadio C.D.T., Castañeda S.S., Cariño F.A., Mendoza N.D.S., 2020. Isotopic data for inferring groundwater dynamics in Cagayan de Oro City, Philippines. *Philippine Journal of Science*, 149(1), 189–199. <https://doi.org/10.56899/149.01.19>.
- Rajendiran T., Sabarathinam C., Chandrasekar T., Panda B., Mathivanan M., Nagappan G., Natesan D., Ghai M., Kumar Singh D., Alagappan R., 2021. Geochemical variations due to salinization in groundwater along the southeast coast of India. *SN Applied Sciences*, 3(5). <https://doi.org/10.1007/s42452-021-04551-2>.
- River Basin Control Office, 2014. Formulation of Integrated River Basin Management and Development Master Plan (IRBMDMP) for Apayao-Abulug River Basin.
- Smedley P.L., Kinniburgh D.G., 2002. A review of the source, behaviour and distribution of arsenic in natural waters. *Applied Geochemistry*, 17, 517–568. [www.elsevier.com/locate/apgeochem](http://www.elsevier.com/locate/apgeochem).
- Stosch H.-G., 2022. Excel template to plot hydrochemical data into a Piper diagram. <https://zenodo.org/records/5994293>.
- Tan S.P.V., Bautista A.T., Mendoza N.D.S., Racadio C.D.T., Puthenpurekal M., Resurreccion A.T., Matsuzaki H., 2020. Iodine-129 for determining the origin of salinity in groundwater in Pampanga, Philippines. *Journal of Environmental Radioactivity*, 218, 106329. <https://doi.org/10.1016/j.jenvrad.2020.106239>.
- Tang M., 2021. Composition of Earth's Crust. In: Alderton, D.H.M., Elias, S.A. (eds.). *Encyclopedia of Geology Volume V*, 2<sup>nd</sup> edition. Academic Press, Cambridge, Massachusetts, United States, 178–186.
- Todd D.K., Mays, L.W., 2005. *Ground water Hydrology* (3<sup>rd</sup> edition). John Wiley and Sons, Inc., New York, USA, 589–608.
- Torres A.D., Lutgardo L., Puthenpurekal M., Boston F., Gomez R., Gatdula A., Guzman J., Urgel V., 2011. Progress report on the groundwater resources and vulnerability assessment of Pampanga Province. Mines and Geosciences Bureau, Department of Environment and Natural Resources, Quezon City, Philippines.
- Ukotije-Ikwut P.R., Steiner Z., Gledhill M., Müller M., Oakes J.M., Sukri R.S., Jiang S., Achterberg E.P., 2023. The distribution and behaviour of Fe, Al, Si, Mn, Cu and Ni in ombrotrophic tropical peat draining blackwater estuaries on Borneo Island. *Frontiers in Marine Science*, 9. <https://doi.org/10.3389/fmars.2022.1075155>.
- Valdez J.D.G., Suggang R.J., Mendoza N.D.S., Racadio C.D.T., Bautista VII A.T., Toya M., Tokuyama H., Yamagata T., Matsuzaki H., 2026. Iodine-129 as an environmental tracer of salinity and freshwater leachates in Boracay Island, Philippines. *Nuclear Instruments and Methods in Physics Research Section B: Beam Interactions with Materials and Atoms*, 571, 165950. <https://doi.org/10.1016/j.nimb.2025.165950>.
- Wallmann K., Geilert S., Scholz F., 2023. Chemical alteration of riverine particles in seawater and marine sediments: Effects on seawater composition and atmospheric CO<sub>2</sub>. *American Journal of Science*, 323. <https://doi.org/10.2475/001c.87455>.
- Yadav K.K., Gupta N., Kumar V., Choudhary P., Khan S.A., 2018. GIS-based evaluation of groundwater geochemistry and statistical determination of the fate of contaminants in shallow aquifers from different functional areas of Agra city, India: Levels and spatial distributions. *RSC Advances*, 8(29), 15876–15889. <https://doi.org/10.1039/C8RA00577J>.